Received: 3 August 2021 | Revised: 23 February 2022 | Accepted: 25 February 2022

DOI: 10.1002/alz.12668

Alzheimer's & Dementia®
THE JOURNAL OF THE ALZHEIMER'S ASSOCIATION

FEATURED ARTICLE

Quantification of amyloid beta and tau PET without a structural MRI

Susan M. Landau[1] | **Tyler J. Ward**[1] | **Alice Murphy**[1] | **Leonardo Iaccarino**[2] | **Theresa M. Harrison**[1] | **Renaud La Joie**[2] | **Suzanne Baker**[3] | **Robert A. Koeppe**[4] | **William J. Jagust**[1,3] | **for the Alzheimer's Disease Neuroimaging Initiative***

[1]Helen Wills Neuroscience Institute, University of California Berkeley, Berkeley, California, USA

[2]Memory and Aging Center, University of California, San Francisco, California, USA

[3]Molecular Biophysics and Integrated Bioimaging, Lawrence Berkeley National Laboratory, Berkeley, California, USA

[4]Division of Nuclear Medicine, University of Michigan, Ann Arbor, Michigan, USA

Correspondence
Susan M. Landau, Helen Wills Neuroscience Institute, University of California Berkeley, 118 Barker Hall, MC 3190, Berkeley, CA 94720-3190, USA.
E-mail: slandau@berkeley.edu

*Data used in preparation of this article were obtained from the Alzheimer's Disease Neuroimaging Initiative (ADNI) database (adni.loni.usc.edu). As such, the investigators within the ADNI contributed to the design and implementation of ADNI and/or provided data but did not participate in analysis or writing of this report. For a complete listing of ADNI investigators, see: https://adni.loni.usc.edu/wpcontent/uploads/how_to_apply/ADNI_Authorship_List.pdf

Funding information
Alzheimer's Disease Neuroimaging Initiative (ADNI); National Institutes of Health, Grant/Award Number: U01 AG024904; Department of Defense ADNI, Grant/Award Number: W81XWH-12-2-0012

Abstract

Introduction: Relying on magnetic resonance imaging (MRI) for quantification of positron emission tomography (PET) images may limit generalizability of the results. We evaluated several MRI-free approaches for amyloid beta (Aβ) and tau PET quantification relative to MRI-dependent quantification cross-sectionally and longitudinally.

Methods: We compared baseline MRI-free and MRI-dependent measurements of Aβ PET ([18F]florbetapir [FBP], N = 1290, [18F]florbetaben [FBB], N = 290) and tau PET ([18F]flortaucipir [FTP], N = 768) images with respect to continuous and dichotomous agreement, effect sizes of Aβ+ impaired versus Aβ– unimpaired groups, and longitudinal standardized uptake value ratio (SUVR) slopes in a subset of individuals.

Results: The best-performing MRI-free approaches had high continuous and dichotomous agreement with MRI-dependent SUVRs for Aβ PET and temporal flortaucipir (R^2 ≥0.95; ± agreement ≥92%) and for Alzheimer's disease–related effect sizes; agreement was slightly lower for entorhinal flortaucipir and longitudinal slopes.

Discussion: There is no consistent loss of baseline or longitudinal AD-related signal with MRI-free Aβ and tau PET image quantification.

KEYWORDS
Alzheimer's disease, amyloid positron emission tomogrraphy, florbetaben, florbetapir, flortaucipir

1 | INTRODUCTION

Quantitative amyloid beta (Aβ) and tau positron emission tomography (PET) imaging measurements are used frequently to assess the degree of pathology burden in vivo in Alzheimer's disease (AD) research and clinical trials of therapeutic treatments. Food and Drug Administration approval of several Aβ PET tracers over the last decade has expanded the reach of PET imaging as a tool in diagnosis of dementia, and the recent approval of aducanumab may further its clinical application. Current clinical use relies on visual reads, but such qualitative examination of images limits detection of subtle and/or regionally specific accumulation of Aβ[1] and tau[2] that are of increasing interest in clinical trials. Quantitative PET image analysis enables detection of such subthreshold accumulation, but the computationally intensive nature of this analysis makes implementation across a variety of clinical and research settings challenging. Measurement of PET standardized

uptake value ratios (SUVRs) often relies on the use of a coregistered structural magneticre sonance imaging (MRI) and specialized software for precise anatomical information used to define regions of interest and reference regions in native space. This precise regional definition may be especially critical for tau PET, because tau accumulates in small medial temporal regions that are vulnerable to noise during transformation into template space. However, the requirement of a recent MRI for PET image quantification excludes PET data when an MRI is unavailable due to expense, participant burden, or an image acquisition problem or contraindication. Requiring an MRI may exclude those with conditions like claustrophobia or medical implants such as pacemakers, thus biasing samples. Inclusion of such individuals contributes to the generalizability of an imaging sample relative to the population.

While "MRI-free" image quantification methods have been developed for cross-sectional Aβ PET[3–7] and, to a lesser extent, tau PET,[8] sample sizes have been limited in some cases, longitudinal data have not been reported, and there is little data on the loss of sensitivity for these approaches compared to MRI-dependent, native space approaches.

The goal of this study was to examine several template-space, MRI-free Aβ and tau PET quantification approaches in relation to a well-validated native space, MRI-dependent approach[9–11] that has been implemented in several multisite studies with data currently available to the scientific community.[12,13] We took advantage of extensive cross-sectional and longitudinal Aβ PET ([18F]florbetapir [FBP], [18F]florbetaben [FBB]) and tau PET ([18F]flortaucipir [FTP]) data from the Alzheimer's Disease Neuroimaging Initiative (ADNI) to create tracer-specific templates for spatial normalization of PET images into standardized (Montreal Neurological Institute [MNI]-152) space without the use of an MRI. We then implemented several approaches for defining regions in MNI space and compared these MRI-free SUVRs to our corresponding "gold standard" MRI-dependent SUVRs. Finally, to examine the practical utility of MRI-free measurements, we compared MRI-free and MRI-dependent measures with respect to (1) agreement between dichotomous (±) Aβ and tau status (2) longitudinal Aβ and tau PET slopes, and (3) tau PET effect sizes of Aβ+ impaired versus Aβ− unimpaired subjects.

RESEARCH IN CONTEXT

1. **Systematic Review**: We used PubMed to identify publications examining quantification methods for amyloid positron emission tomography (PET) imaging.
2. **Interpretation**: This study identifies baseline and longitudinal amyloid and tau PET quantification approaches that do not rely on magnetic resonance imaging (MRI) and compares them to a gold standard MRI-dependent approach. Optimized MRI-free quantification did not involve a clear reduction in Alzheimer's disease (AD)-related signal relative to MRI-dependent baseline and longitudinal quantification of amyloid tracers and tau. This MRI-free approach increases the generalizability of samples with unavailable MRIs or individuals with MRI contraindications.
3. **Future Directions**: The MRI-free data and tools developed in this study are part of an effort in our laboratory to make multisite PET data accessible to the scientific community for use in research and planning clinical trials. This approach can be implemented in a variety of longitudinal, multisite PET studies involving both amyloid and tau PET images.

2 | METHODS

2.1 | Participants

We identified 1589 ADNI participants who had at least a baseline Aβ PET and MRI. Of this group, nine participants were excluded due to receiving different Aβ PET ligands over time (N = 8) or failed spatial normalization (N = 1).

All study data was downloaded from the ADNI database (adni.loni.usc.edu). The ADNI was launched in 2003 as a public–private partnership, led by Principal Investigator Michael W. Weiner, MD. The primary goal of ADNI has been to test whether serial MRI, PET, other biological markers, and clinical and neuropsychological assessment can be combined to measure the progression of MCI and early AD. ADNI has been approved by the local institutional review boards, and all participants signed an informed consent form.

All participants had a baseline MRI and a baseline Aβ PET scan (FBP, N = 1290, FBB, N = 290); 49% (N = 768) had a baseline FBP tau PET scan (Table 1B). Aβ status that was closest in time to the baseline tau PET scan (which may have differed from baseline Aβ status) was used in tau PET analyses. The time interval between the MRI and the baseline PET was within 4 months for 96% of PET scans and 1.1 ± 1.3 years for the remaining scans.

The amount of longitudinal data available for different tracers was variable. Of participants who had FBP PET, 63% of participants had at least 1 follow-up Aβ PET scan, and 36% had three or more follow-up scans; 35% of participants with baseline FTP had at least one follow-up tau PET scan. We did not examine longitudinal FBB data because < 100 subjects had more than one FBB scan.

2.2 | PET and MR image acquisition

PET were acquired (FBP: 10.0 mCi, 4 × 5 minutes frames, 50 to 70 minutes post-injection; FBB: 8.1 mCi, 4 × 5 minutes frames, 90 to 110 minutes; FTP: 10.0 mCi, 6 × 5 minutes frames, 75 to 105 minutes), pre-processed,[14] downloaded from the Laboratory of Neuro Imaging (LONI), and coregistered to the structural MR image closest in time to the baseline PET scan.

TABLE 1 Amyloid beta (Aβ) and tau positron emission tomography (PET) regions of interest for each image processing method

		Aβ			Tau			
			Reference regions		Target regions		Reference regions	
		Target region Cortical summary region	Whole cerebellum	Composite (longitudinal)	Entorhinal cortex	Temporal metaROI	Cerebellar cortex	Eroded subcortical WM (longitudinal)
MRI-dependent	Native space FS ROIs	Frontal, temporal, parietal, cingulate regions	Cerebellar GM + WM	Whole cerebellum, brainstem, eroded WM	Entorhinal cortex	Amygdala, entorhinal cortex, fusiform gyrus, inferior and middle temporal gyri (Supp Methods[9])	Inferior cerebellar cortex[13]	Eroded subcortical WM[13,14]
MRI-free	ADNI200 FS ROIs	Frontal, temporal, parietal, cingulate regions	Cerebellar GM + WM	Whole cerebellum, brainstem, eroded WM	Entorhinal cortex	Amygdala, entorhinal cortex, fusiform gyrus, inferior and middle temporal gyri (Supp Methods[9])	Inferior cerebellar cortex[13]	Eroded subcortical WM[13,14]
	CL ROIs	Frontal, temporal, parietal, precuneus, anterior striatum, insula[15]	MNI152 MR-defined whole cerebellum truncated below z = -52 mm and above -15 mm[15]	No CL version; used ADNI200 FS-defined composite region				
	CVS35 ROIs				Entorhinal cortex	Amygdala, entorhinal cortex, fusiform gyrus, inferior and middle temporal gyri (Supp Methods[9])	Inferior cerebellar cortex[13]	Eroded subcortical WM[13,14]

Abbreviations: ADNI, Alzheimer's Disease Neuroimaging Initiative; CL, Centiloid; GM, gray matter; FS, FreeSurfer; MRI, magnetic resonance imaging; ROI, region of interest; WM, white matter.

2.3 | MRI-dependent pipeline

MRIs were processed with FreeSurfer (FS) v7.1.1 and the resulting regional parcellations from the Desikan-Killiany (DK) atlas[16] were used to define Aβ– and tau-specific target and reference regions used in this study (Table 1) as described previously.[17,18]

For longitudinal Aβ PET analyses, we used a previously validated[19,20,15,21] composite reference region made up of whole cerebellum, brainstem, and eroded subcortical white matter (WM) generated by smoothing native space subcortical WM by 8 mm^3 and thresholding at 0.70.

Tau analysis regions (Table 1) included entorhinal cortex and a composite temporal region (temporal metaROI [region of interest]) made up of amygdala, entorhinal cortex, fusiform gyrus, inferior and middle temporal gyri.[22] The inferior cerebellar cortex reference region is defined by the intersection of the FS-defined cerebellar gray matter (GM; FSregions 8, 47) and the "spatially unbiased atlas template" (SUIT) inferior cerebellum (regions 6, 8–28, 33, 34)[23] that is reverse-normalized back to native space.[11,24] An eroded subcortical WM reference region was used for longitudinal measurements.[25,26]

The MRI closest to the baseline PET scan was used to define ROIs for all longitudinal Aβ and tau SUVRs.

2.4 | MRI-free pipeline

2.4.1 | PET templates

Each native space PET image was warped to MNI space using the appropriate tracer-specific PET template target prior to sampling from the images to generate MRI-free SUVRs.

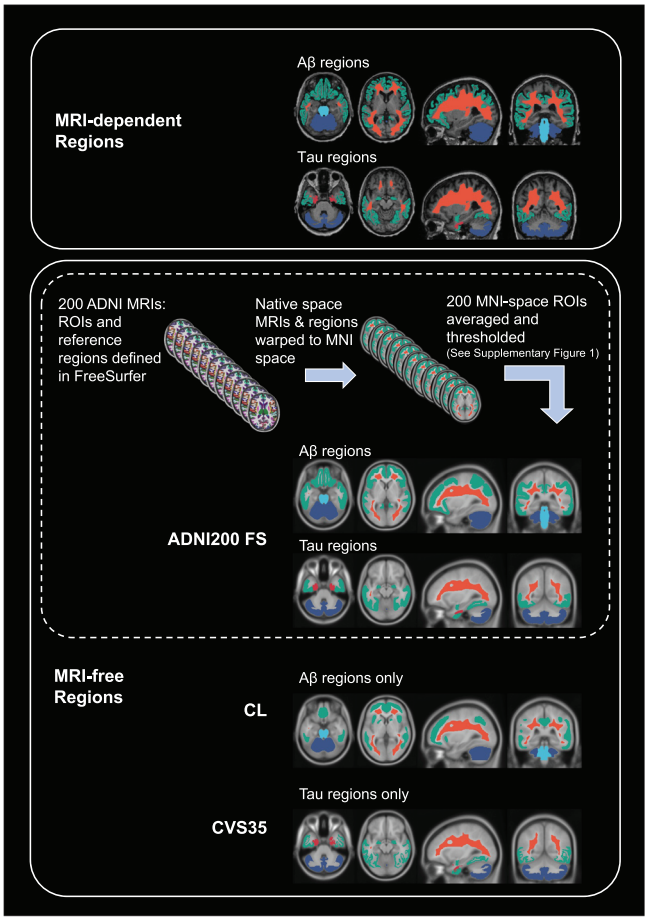

FIGURE 1 Amyloid beta (Aβ) and tau positron emission tomography (PET) templates. PET templates in Montreal Neurological Institute (MNI) space were created for each tracer using a subset of Alzheimer's Disease Neuroimaging Initiative (ADNI) scans (see Methods section). The color bar represents standardized uptake value ratios based on the initial cerebellar cortex intensity normalization applied during ADNI PET pre-processing

Tracer-specific PET templates (Figure 1) were generated with the following steps: (1) FBP, FBB, and FTP scans were randomly selected from 50 Aβ+ impaired, 50 Aβ+ unimpaired, 50 Aβ− impaired, and 50 Aβ− unimpaired ADNI participants. (2) The MRI closest in time to each PET image was spatially normalized to the 1mm T1 template in MNI-152 space using SPM12 (www.fil.ion.ucl.ac.uk/spm). Normalization parameters were applied to the coregistered PET image. (3) Resulting spatially normalized PET images were averaged together to generate each tracer-specific template.

2.4.2 | Overview of candidate MRI-free regions of interest

To determine the variability associated with different methods of defining regions in MNI space, we examined two candidate sets of MNI-space regions for sampling Aβ SUVRs and two candidate sets of MNI-space regions for sampling tau SUVRs.

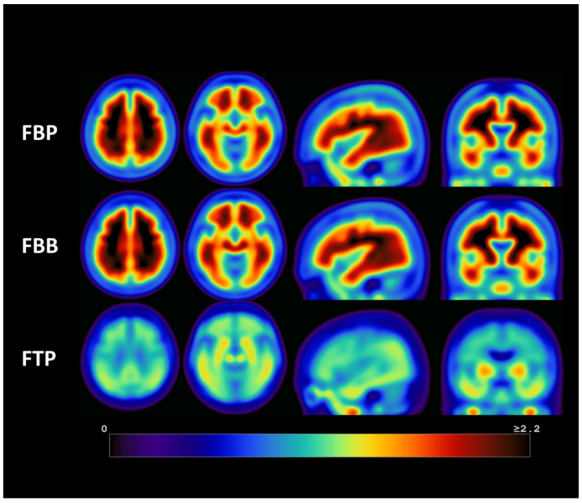

FIGURE 2 Magnetic resonance imaging (MRI)-dependent and MRI-free processing summary. A comparison of MRI-dependent and candidate MRI-free regions (ADNI200 FS, CL, and CVS35; see Methods section) is shown. MRI-dependent amyloid beta (Aβ) and tau regions (top) were based on native-space, FreeSurfer-defined regional parcellations (see Methods section). Aβ and tau-specific regions of interest (green), and cross-sectional (dark blue) and longitudinal reference regions (light blue) are shown for all methods (see Table 1)

2.4.3 | Aβ method 1: ADNI200 FS regions

To develop a template-space atlas made up of 112 DK regions that parallel those used in our native-space, MRI-dependent pipeline, we identified segmented T1 MRIs from a subset of randomly selected 200 cognitively normal (CN) ADNI participants (not the same 200 participants used for PET template definition) using FS. Each binary region in the FS-defined aparc+aseg file was nonlinearly warped to template space, smoothed by 1.5 mm^3 full width half maximum (FWHM), and averaged across the 200 MRIs to create 112 ROI probability maps. Each region probability map was normalized between 0 and 1 (Figure S1A in supporting information) then merged into a single template-space atlas by selecting the highest-ranking ROI for each template space voxel (Figure S1B). From this atlas, we selected ROIs and reference regions for Aβ and tau (Figure 2) were identical to those described in the MRI-dependent methods (above), except that the eroded WM region was thresholded at 0.90 to account for the larger size of this region due to noise introduced during spatial normalization.

2.4.4 | Aβ method 2: Centiloid regions

The Aβ PET MNI-space cortical summary region and a whole cerebellum were downloaded from Global Alzheimer's Association Interactive Network (GAAIN; gaain.org/centiloid-project). These regions were developed and made available for calculating transformation equations for Aβ PET SUVRs across different tracers to a standardized scale Centiloid (CL). The cortical summary region is based on a contrast of [11C]Pittsburgh compound B (PiB) PET images of AD patients versus

controls.[27] The whole cerebellum is truncated to reduce contamination of this region from signal in occipital regions (dorsally) and lack of signal due to low field of view (ventrally). An eroded WM region was not available for the CL pipeline, so we used the ADNI200 FS-defined eroded WM for longitudinal analyses (Table 1).

2.4.5 | Tau method 1: ADNI200 FS regions

We used entorhinal, temporal metaROI, inferior cerebellar cortex, and eroded WM regions defined by FS and warped to MNI space using the same methods as the Aβ ADNI200 FS regions (above).

2.4.6 | Tau method 2: CVS35 regions

Entorhinal and temporal metaROI regions were defined by the combined volumetric and surfaced based MNI-space atlas (CVS35) available in FS. Inferior cerebellar cortex and subcortical WM reference regions were generated using methods that parallel those used in the MRI-dependent and ADNI200 FS pipelines.

2.5 | Statistical analyses

We examined two candidate MNI-space cortical summary regions for Aβ (CL, ADNI200 FS) in relation to MRI-dependent SUVRs. For tau PET, we examined two sets of candidate MNI-space entorhinal and temporal ROIs (CVS35, ADNI200 FS) in relation to MRI-dependent SUVRs. For these comparisons, we examined the linear regression equation (slope, intercept) and correlation (R^2) representing the relationship between continuous MRI-free SUVRs versus MRI-dependent SUVRs and SUVR rates of change using the reference regions listed in Table 1.

To examine agreement in dichotomous (±) Aβ and tau status, we transformed previously validated Aβ and tau MRI-dependent thresholds for each region/tracer into MRI-free "units" using the linear regression equation representing the relationship between MRI-dependent and MRI-free SUVRs. Aβ cortical summary thresholds (FBP: 1.11, FBB: 1.08) were equal to the mean +2 standard deviation (SD) for a sample of young controls, processed using the same MRI-dependent pipeline described here with whole cerebellum normalization.[18] Tau thresholds (entorhinal cortex: 1.23, temporal metaROI: 1.26) were defined by the upper 90th percentile of ADNI Aβ− CN individuals (N = 307; age = 72.7 ± 7.2, edu = 16.8 ± 2.4, 41% female, 27% apolipoprotein E ε4+) and were processed using the same MRI-dependent pipeline described here including inferior cerebellar cortex normalization. We then examined concordance between dichotomous (±) MRI-free and MRI-dependent measures using Cohen's kappa coefficient (k) and percent status agreement.

To evaluate methods for the ability to differentiate AD and non-AD individuals, we compared effect sizes of Aβ+ impaired (MCI, AD) versus Aβ− unimpaired (CN) groups for longitudinal FBP slopes and baseline and longitudinal tau (entorhinal, temporal metaROI) MRI-free versus MRI-dependent SUVrs only (but not baseline Aβ measures to avoid circularity).

3 | RESULTS

3.1 | Sample characteristics

The characteristics of the entire Aβ PET sample (N = 1580; Table 2A) are similar to the characteristics of the subset of individuals who had tau PET (N = 768; Table 2B). There was more available longitudinal data for FBP than FTP, both in terms of the percent of individuals with >1 scan (FBP: 63%, FTP: 35%), and the amount of follow-up time for those individuals with longitudinal data (FBP: 4.5 ± 2.5 years, FTP: 2.2 ± 1.1 years).

3.2 | Aβ MRI-free versus MRI-guided associations

For baseline Aβ PET, both MRI-free cortical summary SUVRs we examined were closely correlated with MRI-guided results (Figure 3A). CL SUVR had the stronger association to MRI-dependent SUVRs for both FBP and FBB, whereas ADNI200 MRI-free SUVRs had a lower slope, indicating a lower dynamic range of values than CL MRI-free SUVRs. The variability of MRI-free versus MRI-dependent SUVRs was more consistent for CL SUVRs across the dynamic range, whereas ADNI200 FS SUVRs underestimated MRI-guided SUVRs for individuals with the highest Aβ burden (Bland-Altman plots; Figure S2 in supporting information).

Both MRI-free methods had strong agreement with MRI-dependent ± status (91% to 94% agreement). The two methods had similar performance but there was slightly higher agreement for CL-defined status (FBP: 94.3%, k = 0.89; FBB: 93.1%, k = 0.86) than for ADNI200-defined status (FBP: 93.6%, k = 0.87; FBB: 91.4%, k = 0.83). Exclusion of cases within a ± 5% "ambiguous range" of the MRI-dependent threshold resulted in even higher agreement with MRI-dependent ± status for both methods (CL: 97.6% for FBP, 95.6% for FBB; ADNI200: 96.7% for FBP, 93.1% for FBB; Table S2 in supporting information).

3.3 | Aβ MRI-free SUVR to CL conversion

Because the CL approach was the best-performing MRI-free method, we calculated conversion equations to CLs for both FBP and FBB to enable standardization of MRI-free SUVRs across tracers.[27] Our MRI-dependent thresholds (FBP: 1.11, FBB: 1.08) correspond to 20 CL (FBP) and 18 CL (FBB) using previously derived MRI-dependent conversions[18] and here our MRI-free, CL method SUVRs converted to 27 for FBP and 22 for FBB (see Supplementary Methods in supporting information).

3.4 | Tau MRI-free versus MRI-dependent associations

Both MRI-free approaches were closely correlated with MRI-guided results, although associations for entorhinal cortex were lower (R^2 = 0.83–0.88) than for the temporal metaROI (R^2 = 0.96–0.97; Figure 3B).

TABLE 2 Amyloid beta (Aβ) and tau positron emission tomography (PET) participant summary

A. Participants with Aβ PET			B. Participants with tau PET	
	Florbetapir	Florbetaben		Flortaucipir
N	1290	290	N	768
Diagnosis			Diagnosis	
CN	38%	56%	CN	55%
MCI	45%	33%	MCI	33%
AD	17%	11%	AD	12%
Age (SD)	73.7 (7.8)	71.6 (6.9)	Age (SD)	74.1 (7.7)
Education (SD)	16.2 (2.7)	16.6 (2.3)	Education (SD)	16.5 (2.5)
Male	52%	47%	Male	48%
APOE ε4+	43%	38%	*APOE* ε4+	38%
Aβ+	53%	38%	Aβ+	40%
% with FTP	38%	94%	% with FBP/% with FBB	64%/36%
Longitudinal timepoints			Longitudinal timepoints	
2 pts	26%		2 pts	16%
3 pts	15%		3 pts	15%
≥4 pts	21%		≥4 pts	4%
Σ	63%		Σ	35%
Longitudinal follow-up (years)	4.5 (2.5)		Longitudinal follow-up (years)	2.1 (1.1)

Abbreviations: AD, Alzheimer's disease; *APOE*, apolipoprotein E; CN, cognitively normal; FBP, [18F]florbetapir; FBB, [18F]florbetaben; FTP, [18F]flortaucipir; MCI, mild cognitive impairment; SD, standard deviation.

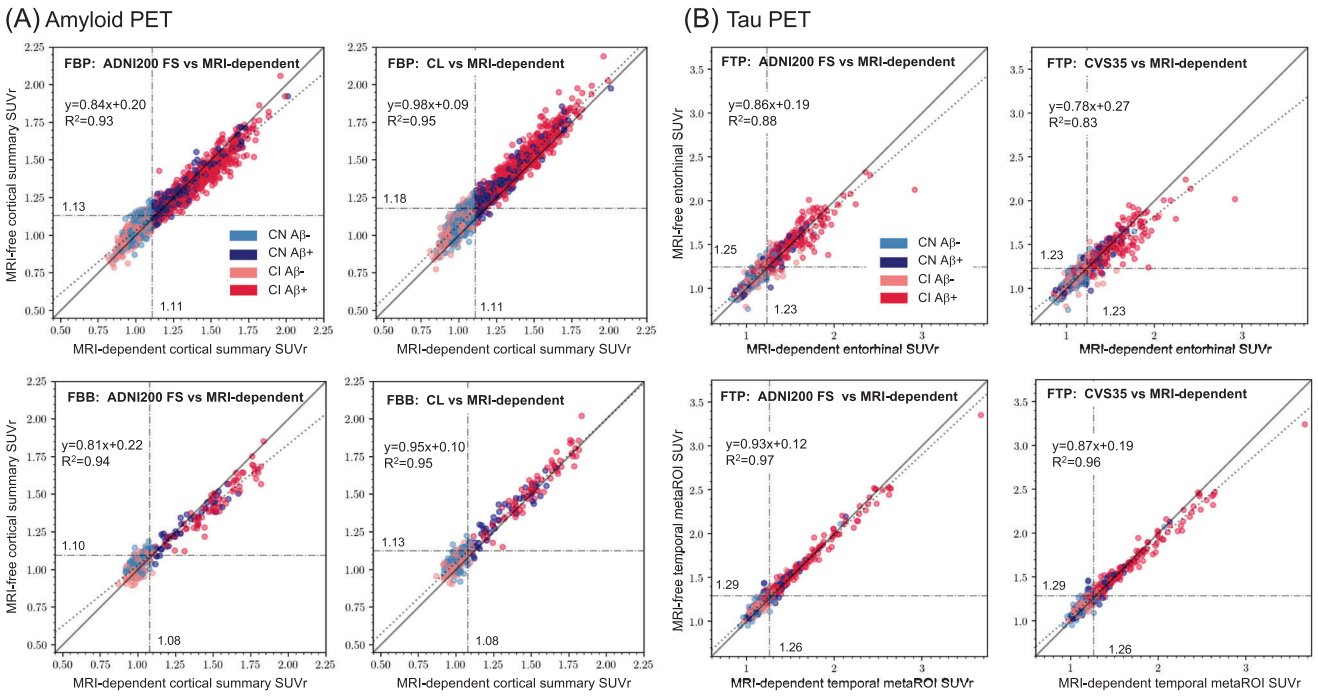

FIGURE 3 Comparison of baseline magnetic resonance imaging (MRI)-dependent versus MRI-free standardized uptake volume ratios (SUVRs). MRI-dependent versus two MRI-free approaches are shown for (A) cortical summary amyloid beta (Aβ) positron emission tomography (PET) ([18F]florbetapir [FBP], [18F]florbetaben [FBB]; whole cerebellum reference) and for (B) tau PET (entorhinal cortex and temporal metaROIs [regions of interest]; cerebellar cortex reference). For each comparison, previously validated thresholds for MRI-dependent SUVRs are shown on the x-axis, and the corresponding MRI-free corresponding thresholds are shown on the y-axis. The line of identity is a solid line; the best-fit linear regression line is dotted. Cognitively normal (CN) and cognitively impaired (CI; mild cognitive impairment or Alzheimer's disease) individuals and Aβ status are represented by the colors shown

TABLE 3 Tau positron emission tomography (PET) effect size comparisons

Region of interest	Reference region	Pipeline	Mean SUVRs		Cohen's d	95% CI	*P*
			Aβ− CU	Aβ+ CI			
Braak1	Cerebellar cortex	MRI-dependent	1.125 (0.104)	1.493 (0.299)	1.67	1.66–1.68	<.001
		ADNI200 FS	1.155 (0.105)	1.494 (0.261)	1.72	1.71–1.72	<.001
		CVS35 FS	1.414 (0.105)	1.440 (0.245)	1.60	1.59–1.60	<.001
Temporal MetaROI	Cerebellar cortex	MRI-dependent	1.180 (0.090)	1.555 (0.411)	1.28	1.27–1.28	<.001
		ADNI200 FS	1.211 (0.098)	1.567 (0.378)	1.30	1.30–1.31	<.001
		CVS35 FS	1.212 (0.097)	1.544 (0.352)	1.30	1.30–1.31	<.001
Braak1	Eroded WM	MRI-dependent	0.970 (0.082)	1.197 (0.189)	1.56	1.55–1.57	<.001
		ADNI-200 FS	1.015 (0.087)	1.266 (0.196)	1.68	1.67–1.68	<.001
		CVS35 FS	1.001 (0.088)	1.234 (0.197)	1.54	1.53–1.55	<.001
Temporal MetaROI	Eroded WM	MRI-dependent	1.018 (0.071)	1.233 (0.214)	1.37	1.36–1.37	<.001
		ADNI200 FS	1.064 (0.083)	1.320 (0.246)	1.41	1.40–1.42	<.001
		CVS35 FS	1.063 (0.087)	1.317 (0.246)	1.39	1.39–1.40	<.001

Abbreviations: 95% CI, confidence interval; Aβ, amyloid beta; ADNI, Alzheimer's Disease Neuroimaging Initiative; CI, cognitively impaired; CU, cognitively unimpaired; FS, FreeSurfer; MRI, magnetic resonance imaging; ROI, region of interest; SUVR, standardized uptake value ratio; WM, white matter.

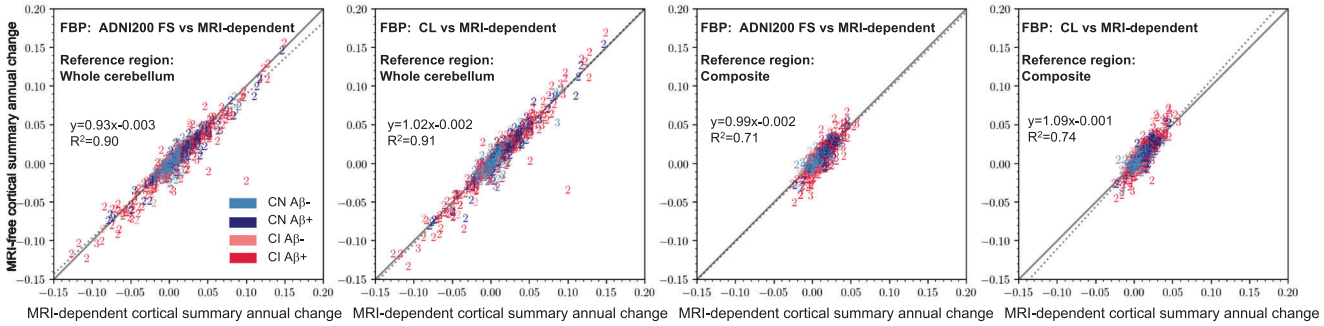

FIGURE 4 Comparison of longitudinal amyloid beta (Aβ) magnetic resonance imaging (MRI)-dependent versus MRI-free standardized uptake volume ratio (SUVR) slopes. MRI-dependent versus two MRI-free approaches are shown for annualized SUVR slopes calculated using the whole cerebellum (left two plots) or composite reference region (right two plots). The line of identity is a solid line; the best-fit linear regression line is dotted. The number of timepoints used to calculate the annualized slopes are used as point labels

Performance of the two MRI-free methods we examined (ADNI200 and CVS35) was similar. The ADNI200 SUVrRs had the stronger association to MRI-dependent SUVRs across both regions and larger dynamic range of values (slopes). Both sets of MRI-free SUVRs underestimated MRI-guided SUVRs for individuals with the highest tau, but this underestimation was slightly less severe for the ADNI200 SUVRs (Bland-Altman plots; Figure S3 in supporting information).

Finally, ± status agreement for both MRI-free methods was highly concordant with MRI-dependent ± status (89% to 92% agreement). Status agreement was slightly higher for ADNI200-defined status (entorhinal: 90.4%, k = 0.79; temporal: 92.4%, k = 0.83) than for CVS35-defined status (entorhinal: 89.1%, k = 0.76; temporal: 91.1%; k = 0.80). Exclusion of cases within a ± 5% "gray zone" of the MRI-dependent threshold resulted in even higher agreement with MRI-dependent ± status for both regions (ADNI200 FS: 94%).

A comparison of effect sizes for MRI-dependent and MRI-free SUVRs (Table 3) showed that there was no clear advantage of the MRI-dependent pipeline over the best-performing MRI-free pipeline (ADNI200 FS) for either entorhinal or temporal regions or for either reference region. In fact, the effect sizes for the ADNI200 FS SUVRs were numerically higher than the MRI-dependent effect sizes in each case. Also, consistent with the continuous and dichotomous SUVR findings, the ADNI200 FS entorhinal SUVRs outperformed the CVS35 SUVRs.

3.5 | Longitudinal Aβ MRI-free versus MRI-dependent associations

MRI-dependent FBP slopes were highly correlated with MRI-free slopes across both MRI-free methods (Figure 4; Figure S4 in supporting information). The MRI-dependent effect sizes were higher than both MRI-free effect sizes (Table 4), and the CL method longitudinal effect sizes were slightly larger than the ADNI200 FS longitudinal effect sizes.

TABLE 4 Longitudinal β-amyloid (Aβ) positron emission tomography (PET) effect size comparisons

Region of interest	Reference region	Pipeline	Mean annual SUVR change		Cohen's d	95% CI	P
			Aβ− CU	Aβ+ CI			
Cortical summary	Whole cerebellum	MRI-dependent	0.003 (0.015)	0.009 (0.042)	0.17	0.16–0.18	.056
		ADNI200 FS	0.001 (0.015)	0.002 (0.041)	0.06	0.05–0.06	.492
		CL	0.002 (0.017)	0.006 (0.045)	0.12	0.11–0.12	.172
Cortical summary	Composite	MRI-dependent	0.002 (0.008)	0.010 (0.014)	0.65	0.64–0.65	<.001
		ADNI200 FS	0.001 (0.008)	0.006 (0.018)	0.34	0.33–0.34	<.001
		CL[a]	0.002 (0.009)	0.009 (0.020)	0.44	0.43–0.45	<.001

[a]The ADNI200 eroded WM region was used in the composite reference region for CL pipeline.
Abbreviations: 95% CI, confidence interval; Aβ, amyloid beta; ADNI, Alzheimer's Disease Neuroimaging Initiative; CI, cognitively impaired; CL, Centiloid; CU, cognitively unimpaired; MRI, magnetic resonance imaging; SUVR, standardized uptake value ratio; WM, white matter.

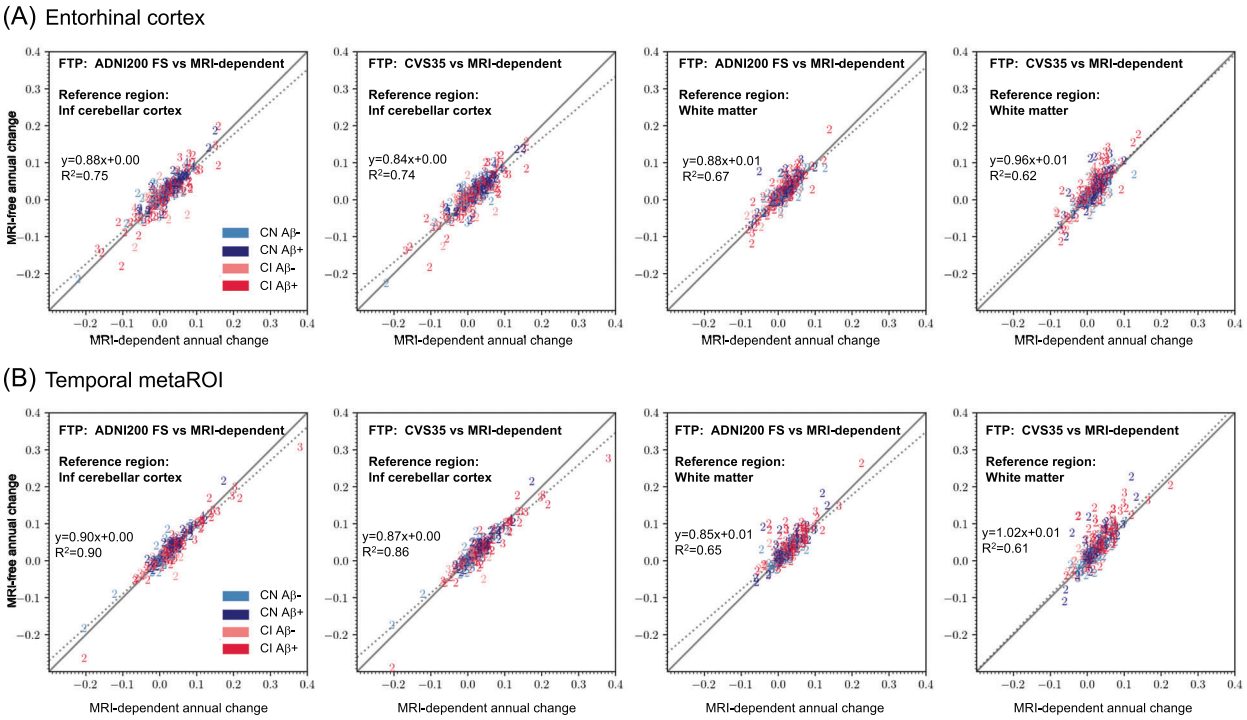

FIGURE 5 Comparison of longitudinal tau magnetic resonance imaging (MRI)-dependent versus MRI-free standardized uptake volume ratio (SUVR) slopes. MRI-dependent versus two MRI-free approaches are shown for (A) annualized entorhinal SUVR slopes and (B) temporal metaROI (region of interest) SUVR slopes, calculated using cerebellar cortex (left) or eroded white matter reference regions (right). The line of identity is a solid line; the best-fit linear regression line is dotted. The number of timepoints used to calculate the annualized slopes are used as point labels

There was also a strong effect of reference region on slopes such that the dynamic range of slopes and corresponding correlations were higher for slopes using whole cerebellar intensity normalization (Figure 4, left) compared to the composite reference region (Figure 4, right), but composite-based slopes had substantially larger effect sizes across all pipelines (Table 4).

3.6 | Longitudinal tau MRI-free versus MRI-dependent associations

The longitudinal and baseline FTP relationships were consistent in that MRI-free versus MRI-dependent associations and effect sizes (Figure 5, Table 5) were lower for the entorhinal slopes than for the temporal metaROI slopes; in fact, entorhinal slope effect sizes reflected no significant differences between groups. For the temporal slope effect sizes, the ADNI200 FS and CVS35 performance was extremely similar. ADNI200 FS performed slightly better than CVS35 slopes with inferior cerebellar cortex intensity normalization; with eroded WM normalization, CVS35 had a slight advantage.

Like FBP slopes, FTP slopes with WM-containing reference had a reduced dynamic range than slopes with cerebellar cortex reference (Figure 5, Figure S5 in supporting information), but there was a less consistent influence of reference region on effect sizes of the slopes than there was for FBP (Table 5). The MRI-dependent pipeline outperformed the MRI-free pipelines *only* with cerebellar intensity

TABLE 5 Longitudinal tau positron emission tomography (PET) effect size comparisons

Region of interest	Reference region	Pipeline	Mean annual SUVR change		Cohen's d	95% CI	*P*
			Aβ- CU	Aβ+ CI			
Braak1	Cerebellar cortex	MRI-dependent	0.004 (0.046)	0.007 (0.065)	0.05	0.05–0.06	.658
		ADNI200 FS	0.005 (0.036)	0.000 (0.068)	−0.09	−0.09–0.08	.552
		CVS35 FS	0.002 (0.038)	0.000 (0.064)	−0.05	−0.06–0.04	.764
Temporal MetaROI	Cerebellar cortex	MRI-dependent	0.005 (0.044)	0.040 (0.074)	0.60	0.59–0.61	<.001
		ADNI200 FS	0.004 (0.033)	0.033 (0.069)	0.56	0.55–0.57	<.001
		CVS35 FS	0.003 (0.033)	0.030 (0.068)	0.53	0.51–0.54	.001
Braak1	Eroded WM	MRI-dependent	0.010 (0.024)	0.008 (0.043)	−0.034	−0.04–0.02	.800
		ADNI200 FS	0.012 (0.023)	0.013 (0.050)	0.032	0.02–0.04	.852
		CVS35 FS	0.011 (0.024)	0.015 (0.048)	0.103	0.09–0.11	.492
Temporal MetaROI	Eroded WM	MRI-dependent	0.01 (0.023)	0.035 (0.040)	0.78	0.77–0.79	<.001
		ADNI200 FS	0.011 (0.022)	0.043 (0.043)	0.95	0.94–0.96	<.001
		CVS35 FS	0.012 (0.022)	0.043 (0.039)	1.01	1.00–1.02	<.001

Abbreviations: 95% CI, confidence interval; Aβ, amyloid beta; ADNI, Alzheimer's Disease Neuroimaging Initiative; CI, cognitively impaired; CU, cognitively unimpaired; FS, FreeSurfer; MRI, magnetic resonance imaging; ROI, region of interest; SUVR, standardized uptake value ratio; WM, white matter.

normalization, but the MRI-free pipelines outperformed the MRI-dependent pipeline with eroded WM reference.

3.7 | Associations between pipeline discrepancy and hippocampal volume

To estimate the influence of atrophy on pipeline agreement, we examined the extent to which differences in MRI-free versus MRI-dependent cross-sectional SUVRs were associated with adjusted hippocampal volumes (Figure S6 in supporting information). The poorer performing ADNI200 FS MRI-free pipeline underestimated FBP SUVRs as hippocampal volumes decreased, whereas the CL pipeline did not, suggesting that the CL pipeline was less vulnerable to atrophy-driven error. For temporal tau, the ADNI200 FS and CVS35 pipelines were both slightly vulnerable to atrophy, but this relationship was more pronounced for the CVS35 regions.

4 | DISCUSSION

The goal of this study was to optimize quantification of cross-sectional and longitudinal Aβ and tau PET images from a large multisite sample without the use of a structural MRI. We examined several candidate MRI-free strategies using cross-sectional and longitudinal PET data acquired with three tracers from the large multisite ADNI sample. We identified optimal MRI-free approaches for Aβ and tau separately using several methods of evaluation in relation to MRI-dependent SUVRs processed using more rigorously defined anatomical information. The best-performing MRI-free approaches were highly correlated with the MRI-dependent results for both continuous and dichotomous comparisons (Aβ PET: 93% to 94% ± agreement; tau PET: 90% to 92% ± agreement). Notably, while the AD-related effect size comparisons revealed a small advantage of the MRI-dependent pipeline for longitudinal Aβ and longitudinal tau (cerebellar cortex reference only), for baseline and longitudinal tau with WM reference, there was no consistent advantage of the MRI-dependent pipeline over the best-performing MRI-free pipeline, even for entorhinal cortex.

For Aβ PET, the CL region was the best-performing MNI space approach relative to MRI-dependent SUVRs based on broader dynamic ranges, higher correlations, and larger effect sizes compared to the CVS35 approach. A key difference between the two approaches was that the ADNI200 FS cortical summary region was more lateral and closer to the gray matter/cerebrospinal fluid (CSF) border, whereas the CL region was closer to the gray matter/white matter border. While the CL region was vulnerable to contamination by off-target binding in white matter, this contamination played a smaller role than the SUVR-lowering effect of CSF signal on the ADNI200 FS region, which resulted in disproportionately lower ADNI200 FS SUVRs with greater Aβ burden, and therefore a reduced dynamic range relative to MRI-guided SUVRs. The slope effect sizes were higher for the MRI-dependent than CL SUVRs across both reference regions. However, across pipelines, effect sizes of slopes with a WM-containing reference were considerably higher than effect sizes of slopes with whole cerebellum reference, consistent with previous findings.[19,20,15,21]

For tau PET, the two MRI-free approaches performed similarly but the ADNI200 FS approach had slightly higher dynamic ranges and correlations with MRI-dependent SUVRs cross-sectionally, especially for baseline entorhinal FTP. Both MRI-free approaches performed similarly with respect to entorhinal and temporal slopes. Associations with continuous MRI-dependent SUVRs and SUVR slopes were higher for the temporal metaROI than for entorhinal cortex, likely due to the small size of the entorhinal region, but ± agreement was similar across both

regions (90% to 92%). Reference region selection (cerebellar cortex, eroded WM) played a less consistent role in influencing slope correlations or effect sizes compared to FBP. The ADNI200 FS regions may have outperformed the CVS35 regions for entorhinal cortex SUVRs because the atlas was generated using an older sample (a subset of ADNI participants) which may have captured signal in the region more accurately, making it less vulnerable to atrophy-driven partial volume effects (Figure S6).

Even though ± status agreement was generally high, there were cases with SUVR discrepancies between MRI-free and MRI-dependent methods (deviations from the regression line). The entorhinal cortex was particularly susceptible to such discrepancies due to its size. An examination of individual outliers suggested that the reason for the discrepancies in the MRI-dependent and MRI-free relationship was inconsistent and could be accounted for by problems with either FS regional definition or spatial normalization.

Analysis of PET data without the aid of an MRI may be necessary for several practical reasons. MRI scans are often obtained in Aβ and tau PET research studies and clinical trials to rule out clinically significant neurological abnormalities or characteristics that would affect image quantification, but requirement of such an MRI adds to the study cost and excludes participants with MRI contraindications such as claustrophobia, medical or dental implants, or metal embedded in the body. Exclusion of such participants may limit generalizability and contribute to discrepant outcomes reported in clinical trials versus imaging substudies. When some participants are missing MRIs, use of MRI-free analyses described here could successfully replace MRI-dependent analyses with minimal compromise in accuracy. Alternatively, MRI-free SUVRs for a subset of participants could be converted into MRI-dependent SUVR "units" using a linear regression equation representing the association between the two methods.

This study extends previous work demonstrating the feasibility of cross-sectional and longitudinal MRI-free quantification PET in a large multisite sample with data and methods available to the scientific community. Previous work has involved cross-sectional data, primarily Aβ PET, and relatively limited samples.[8,4–7] The cross-sectional performance of our Aβ pipeline is highly comparable to MRI-free methods that were recently developed for cross-sectional Aβ PET and validated in several large, multisite datasets with multiple Aβ PET tracers,[3] using similar ROIs. This study reported an overall concordance rate of 94% with MRI-dependent results, which is almost identical to the concordance rate we observed for Aβ PET. We are unaware of other studies that have examined concordance between MRI-free and MRI-dependent cross-sectional or longitudinal tau data, or longitudinal Aβ data. It is striking that many of our effect size comparisons, even for tau PET, showed no clear disadvantage of using MRI-free methods compared to the more rigorous MRI-dependent approach, because MRI-free pipelines like those described in this study are generally considered more vulnerable to noise. This may be because both native space regional definition and MRI-free spatial normalization rely on transformations between native space and MNI space that introduce noise related to deformation in both directions, and this is pronounced in older individuals with atrophy and patients with AD.[28]

There are several key strengths of these findings. These effects are not linked to any particular scanner characteristics or image reconstruction because ADNI image data were collected and merged across many sites using ADNI PET harmonization procedures. The CL regions (the top-performing Aβ MRI-free approach) are sample-independent and widely available, as are the CVS35 regions, and the ADNI200 FS regions and PET templates described here will be made available to the scientific community on the ADNI database alongside existing MRI-dependent quantitative data. In addition, beyond the regions reported in this article, ADNI200 FS and CVS35 templates include a complete set of anatomically defined ROIs that can be used to investigate whole-brain Aβ or tau relationships.

A potential limitation of this work is that the tau MRI-free pipeline was developed using FTP data and our findings may not generalize to use with other tau PET tracers. In addition, the ADNI200 FS regions and PET templates are sample-specific because they were generated using subsets of ADNI participants, although these subsets are large and work in our laboratory suggests that they generalize to other cohorts. The CL approach did not have a complete set of usable regions for all comparisons, so a substitution was made when creating the composite reference region, which could have affected outcomes. Partial volume correction is another analytical process that relies on anatomical information defined by MRI that is sometimes used in our laboratory, particularly for FTP PET quantification,[24] but we chose not to include this comparison because it introduces additional sources of noise that make direct comparison to MRI-free results challenging. Finally, although this article focused on the comparison of different types of regions used to sample data in template space, we did not examine different approaches to MRI-free spatial normalization. Recent work has developed novel approaches for generating target images for PET-only spatial normalization[29] that may improve the performance of the methods described here.

Overall, we identified optimized MRI-free Aβ and tau quantification approaches for cross-sectional and longitudinal quantification that resulted in minimal loss of AD-specific signal compared to MRI-dependent processing. While we do not advocate combining separately processed MRI-free and MRI-dependent SUVRs within the same dataset, an MRI-free pipeline for the entire dataset can be used when MRIs are unavailable for a subset of the sample to increase the generalizability of the sample in populations that include individuals with MRI contraindications. Another option is to transform MRI-free SUVRs into MRI-dependent SUVR "units" using a known linear regression equation representing the association between the two methods. In addition, to generate standardized, tracer-independent findings, FBB and FBP MRI-free SUVRs could be transformed to Centiloids.

ACKNOWLEDGMENTS

Data collection and sharing for this project was funded by the Alzheimer's Disease Neuroimaging Initiative (ADNI; National Institutes of Health Grant U01 AG024904) and DOD ADNI (Department of Defense award number W81XWH-12-2-0012). ADNI is funded by the National Institute on Aging, the National Institute of Biomedical

Imaging and Bioengineering, and through generous contributions from the following: AbbVie; Alzheimer's Association; Alzheimer's Drug Discovery Foundation; Araclon Biotech; BioClinica, Inc.; Biogen; Bristol-Myers Squibb Company; CereSpir, Inc.; Cogstate; Eisai Inc.; Elan Pharmaceuticals, Inc.; Eli Lilly and Company; EuroImmun; F. Hoffmann-La Roche Ltd and its affiliated company Genentech, Inc.; Fujirebio; GE Healthcare; IXICO Ltd.; Janssen Alzheimer Immunotherapy Research & Development, LLC; Johnson & Johnson Pharmaceutical Research & Development LLC; Lumosity; Lundbeck; Merck & Co., Inc.; Meso Scale Diagnostics, LLC; NeuroRx Research; Neurotrack Technologies; Novartis Pharmaceuticals Corporation; Pfizer Inc.; Piramal Imaging; Servier; Takeda Pharmaceutical Company; and Transition Therapeutics. The Canadian Institutes of Health Research is providing funds to support ADNI clinical sites in Canada. Private sector contributions are facilitated by the Foundation for the National Institutes of Health (www.fnih.org). The grantee organization is the Northern California Institute for Research and Education, and the study is coordinated by the Alzheimer's Therapeutic Research Institute at the University of Southern California. ADNI data are disseminated by the Laboratory for Neuro Imaging at the University of Southern California.

ETHICS APPROVAL AND CONSENT TO PARTICIPATE

All participants gave informed consent through their local IRBs prior to study participation.

CONFLICTS OF INTEREST

Susan M. Landau has received travel funding from the Alzheimer's Association and has served on the Scientific Advisory Board and DSMB for KeifeRx. William J. Jagust has served as a consultant to Genentech, Bioclinica, and Biogen. Suzanne L. Baker has served as a consultant to Genentech. Tyler J. Ward, Alice Murphy, Leonardo Iaccarino, Theresa M. Harrison, and Renaud La Joie report no disclosures.

REFERENCES

1. Farrell ME, Jiang S, Schultz AP, et al. Defining the lowest threshold for amyloid-PET to predict future cognitive decline and amyloid accumulation. *Neurology*. 2021;96:e619-e631.
2. Mintun MA, Lo AC, Duggan Evans C, et al. Donanemab in early Alzheimer's disease. *N Engl J Med*. 2021;384:1691-1704.
3. Iaccarino L, La Joie R, Koeppe R, et al. rPOP: robust PET-only processing of community acquired heterogeneous amyloid-PET data. *Neuroimage*. 2022;246:118775.
4. Pegueroles J, Montal V, Bejanin A, et al. AMYQ: an index to standardize quantitative amyloid load across PET tracers. *Alzheimers Dement*. 2021;17(9):1499-1508.
5. Bourgeat P, Villemagne VL, Dore V, et al. Comparison of MR-less PiB SUVR quantification methods. *Neurobiol Aging*. 2015;36(Suppl 1):S159-S166.
6. Edison P, Carter SF, Rinne JO, et al. Comparison of MRI based and PET template based approaches in the quantitative analysis of amyloid imaging with PIB-PET. *Neuroimage*. 2013;70:423-433.
7. Dore V, Bullich S, Rowe CC, et al. Comparison of (18)F-florbetaben quantification results using the standard Centiloid, MR-based, and MR-less CapAIBL((R)) approaches: validation against histopathology. *Alzheimers Dement*. 2019;15:807-816.
8. Fleisher AS, Pontecorvo MJ, Devous MD, Sr., et al. Positron emission tomography imaging with [18F]flortaucipir and postmortem assessment of Alzheimer disease neuropathologic changes. *JAMA Neurol*. 2020;77:829-839.
9. Mormino EC, Smiljic A, Hayenga AO, et al. Relationships between beta-amyloid and functional connectivity in different components of the default mode network in aging. *Cereb Cortex*. 2011;21:2399-2407.
10. Scholl M, Lockhart SN, Schonhaut DR, et al. PET imaging of Tau deposition in the aging human brain. *Neuron*. 2016;89:971-982.
11. Maass A, Landau S, Baker SL, et al. Comparison of multiple tau-PET measures as biomarkers in aging and Alzheimer's disease. *Neuroimage*. 2017;157:448-463.
12. Weiner MW, Harvey D, Hayes J, et al. Effects of traumatic brain injury and posttraumatic stress disorder on development of Alzheimer's disease in Vietnam Veterans using the Alzheimer's disease neuroimaging initiative: preliminary report. *Alzheimers Dement (N Y)*. 2017;3:177-188.
13. Landau SM, Mintun MA, Joshi AD, et al. Amyloid deposition, hypometabolism, and longitudinal cognitive decline. *Ann Neurol*. 2012;72:578-586.
14. ADNI database. ida.loni.usc.edu
15. Chen K, Roontiva A, Thiyyagura P, et al. Improved power for characterizing longitudinal amyloid-beta PET changes and evaluating amyloid-modifying treatments with a cerebral white matter reference region. *J Nucl Med*. 2015;56:560-566.
16. Desikan RS, Segonne F, Fischl B, et al. An automated labeling system for subdividing the human cerebral cortex on MRI scans into gyral based regions of interest. *Neuroimage*. 2006;31:968-980.
17. Landau SM, Mintun M, Joshi A, et al. Amyloid deposition, hypometabolism, and longitudinal cognitive decline. *Ann Neurol*. 2012;72(4):578-586.
18. Royse SK, Minhas DS, Lopresti BJ, et al. Validation of amyloid PET positivity thresholds in centiloids: a multisite PET study approach. *Alzheimers Res Ther*. 2021;13:99.
19. Landau SM, Fero A, Baker SL, et al. Measurement of longitudinal beta-amyloid change with 18F-florbetapir PET and standardized uptake value ratios. *J Nucl Med*. 2015;56:567-574.
20. Brendel M, Hogenauer M, Delker A, et al. Improved longitudinal [(18)F]-AV45 amyloid PET by white matter reference and VOI-based partial volume effect correction. *Neuroimage*. 2015;108:450-459.
21. Fleisher AS, Joshi AD, Sundell KL, et al. Use of white matter reference regions for detection of change in florbetapir positron emission tomography from completed phase 3 solanezumab trials. *Alzheimers Dement*. 2017;13:1117-1124.
22. Jack CR, Jr., Wiste HJ, Weigand SD, et al. Defining imaging biomarker cut points for brain aging and Alzheimer's disease. *Alzheimers Dement*. 2017;13:205-216.
23. Diedrichsen J. A spatially unbiased atlas template of the human cerebellum. *Neuroimage*. 2006;33:127-138.
24. Baker SL, Maass A, Jagust WJ. Considerations and code for partial volume correcting [(18)F]-AV-1451 tau PET data. *Data Brief*. 2017;15:648-657.
25. Harrison TM, La Joie R, Maass A, et al. Longitudinal tau accumulation and atrophy in aging and Alzheimer disease. *Ann Neurol*. 2019;85:229-240.
26. Schwarz CG, Therneau TM, Weigand SD, et al. Selecting software pipelines for change in flortaucipir SUVR: balancing repeatability and group separation. *Neuroimage*. 2021;238:118259.
27. Klunk WE, Koeppe RA, Price JC, et al. The Centiloid Project: standardizing quantitative amyloid plaque estimation by PET. *Alzheimers Dement*. 2015;11:1-15 e1-4.
28. Ishii K, Willoch F, Minoshima S, et al. Statistical brain mapping of 18F-FDG PET in Alzheimer's disease: validation of anatomic standardization for atrophied brains. *J Nucl Med*. 2001;42:548-557.

29. Lilja J, Leuzy A, Chiotis K, Savitcheva I, Sorensen J, Nordberg A. Spatial normalization of (18)F-Flutemetamol PET images using an adaptive principal-component template. *J Nucl Med*. 2019;60:285-291.

SUPPORTING INFORMATION

Additional supporting information may be found in the online version of the article at the publisher's website.

How to cite this article: Landau SM, Ward TJ, Murphy A, et al. Quantification of amyloid beta and tau PET without a structural MRI. *Alzheimer's Dement*. 2023;19:444–455. https://doi.org/10.1002/alz.12668